Tomographic phase microscopy with 180° rotation of live cells in suspension by holographic optical tweezers

Mor Habaza, Barak Gilboa, Yael Roichman, and Natan T. Shaked*

Department of Biomedical Engineering, Faculty of Engineering, Tel-Aviv University, Tel-Aviv 69978, Israel
**Corresponding author: nshaked@tau.ac.il*

Received January 27, 2015; revised March 4, 2015; accepted March 9, 2015;
posted March 11, 2015 (Doc. ID 233236); published April 15, 2015

We present a new tomographic phase microscopy (TPM) approach that allows capturing the three-dimensional refractive index structure of single cells in suspension without labeling, using 180° rotation of the cells. This is obtained by integrating an external off-axis interferometer for wide-field wave front acquisition with holographic optical tweezers (HOTs) for trapping and micro-rotation of the suspended cells. In contrast to existing TPM approaches for cell imaging, our approach does not require anchoring the sample to a rotating stage, nor is it limited in angular range as is the illumination rotation approach. Thus, it allows noninvasive TPM of suspended live cells in a wide angular range. The proposed technique is experimentally demonstrated by capturing the three-dimensional refractive index map of yeast cells, while collecting interferometric projections at an angular range of 180° with 5° steps. The interferometric projections are processed by both the filtered back-projection method and the diffraction theory method. The experimental system is integrated with a spinning disk confocal fluorescent microscope for validation of the label-free TPM results.

OCIS codes: (090.2880) Holographic interferometry; (110.0180) Microscopy; (180.3170) Interference microscopy; (170.6960) Tomography; (170.3010) Image reconstruction techniques; (100.6890) Three-dimensional image processing.
http://dx.doi.org/10.1364/OL.40.001881

The three-dimensional refractive index distribution of biological cells is valuable, since it is related to the structure and to the protein contents of the different cellular organelles and their dynamics. Tomographic phase microscopy (TPM) can measure quantitatively the three-dimensional (3-D) distribution of the refractive index in biological cells [1–8]. This is done by capturing the complex wave fronts of light transmitted through the cell from various angles by using interferometry, and processing these interferometric projections to the three-dimensional refractive index map of the sample.

To measure the wave front transmitted through the cell from multiple angles, previous TPM approaches used either illumination beam rotation [3–7] or sample rotation [1,2,8]. In the first case, the illumination beam rotates, whereas the specimen and the optical setup are stationary. Although this approach does not perturb the sample during data acquisition, the acceptance angle of the illumination is limited, typically to ±70°; therefore, there are missing points in the angular spectrum, which need to be interpolated digitally. In the case of TPM with sample rotation, the assumption is that before the sample the incident wave always propagates with no angle relative to the normal of the detector plane, which was previously obtained by either entire sample rotation [1,8] or patch clamping [2]. In both methods, an external rotation stage is needed while physically holding the sample, which does not allow for noninvasive TPM of cells in suspension.

Optical tweezers provide the capability to create multiple optical traps and to manipulate biological cells in all directions. This technique was previously shown to be noninvasive to live cells while manipulating them [9–11].

Interferometric phase microscopy (IPM) can be used to capture the wave front of the light transmitted through the cell without labeling. [12–14]. Previous works combined optical tweezers and IPM to manipulate biological cells during their quantitative phase imaging [15–20]. Recently, we proposed a portable IPM module that can be connected to the output port of an existing microscope, illuminated by coherent or partially coherent light, and record the complex wave front of the beam transmitted through the sample in a single exposure [13,14].

In the current Letter, we used portable IPM together with holographic optical tweezers (HOTs), to fully (180°) rotate single cells in suspension using multiple, dynamically controlled optical traps, and experimentally measured the three-dimensional refractive index map of the cells. This enables acquisition throughout a wider angular range than in the illumination rotation method, and does not limit the cell environment because of the need to rotate the entire sample or patch clamp the cell.

The proposed experimental setup is shown in Fig. 1. The HOTs setup, with beams marked in red, is combined with an off-axis IPM setup, with beams marked in green, and a spinning disk confocal fluorescent microscopy setup, with beams marked in blue. These three systems are integrated into an upright/inverted microscope (IX, Olympus).

For HOTs, a light beam from an Ytterbium-doped fiber laser (KPS-KILAS-TRAPP 1083-20-PM-CO, Keopsys, wavelength 1083 nm, maximal power 20 W) expands through lenses L1 ($f = 5$ cm) and L2 ($f = 50$ cm) to cover the active area of a liquid crystal spatial light modulator (SLM, X10468-07, Hamamatsu). The SLM generates the desired phase pattern, which eventually induces multiple optical traps on the sample. Lenses L3 ($f = 40$ cm) and L4 ($f = 30$ cm) reduce the beam diameter to overfill the back aperture of microscope objective MO (Olympus PlanApo, 60×, NA = 1.42, oil immersion). This inverted objective lens focuses the beam to create the desired optical trap array [10]. Upon cell trapping, the multiple traps can be moved in the three-dimensional space by digitally controlling the pattern on the SLM in order to rotate the trapped cells on any of the axes. The trap localization precision was 30 nm, leading to a maximum rotation error of 0.7°.

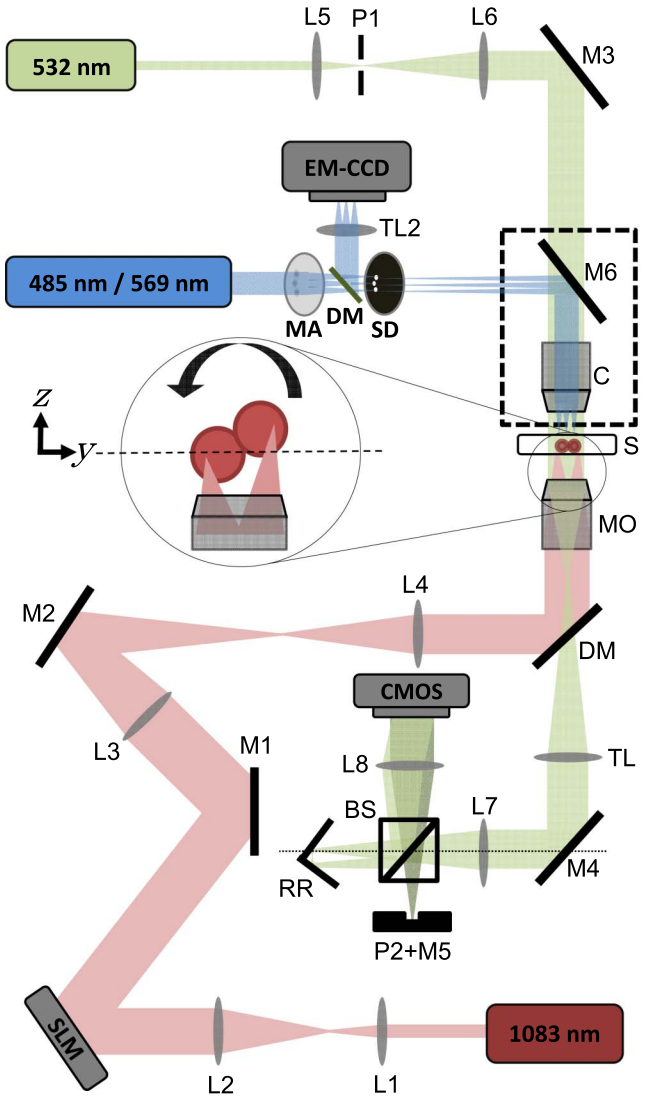

Fig. 1. Optical setup diagram for TPM with full rotation of single cells in suspension. The system combines HOTs (red beams) for cell rotation, external IPM (green beams) for wave front acquisition during the rotation, and spinning disk confocal fluorescent microscopy (blue lines), as a control system. HOTs system components: 1083 nm laser; L1-L4, lenses; SLM, spatial light modulator; M1, M2, mirrors; DM1, dichroic mirror; S, sample, and MO, microscope objective. IPM system components: 532 nm laser, L5-L8, lenses; P1,P2, pinholes; S, sample, MO, microscope objective; DM1, dichroic mirror; TL1, tube lens; M4, M5, mirrors; BS, beam splitter; RR, two-mirror retro-reflector; CMOS digital camera. Spinning disk confocal microscopy system components: 488 nm or 561 nm laser; MA, microlens array; PD, pinhole disk; M6, mirror; C, condenser; S, sample; DM2, dichroic mirror; EF, emission filter; TL2, tube lens; and EM-CCD digital camera.

The upper part of the system shown in Fig. 1 consists of the light sources for either IPM or confocal microscopy modes. When using IPM, as opposed to confocal microscopy, mirror M6 and condenser lens C, marked with a dashed box, are removed. In the IPM system, we used a 532 nm wavelength diode-pumped laser (Compass 2158M-50, Coherent) in the input of the inverted microscope in transmission mode. The illumination beam is filtered and expanded through lenses L5 ($f = 3$ cm) and L6 ($f = 20$ cm) and pinhole P1 (diameter of 75 μm). The compact off-axis τ interferometer [14] was connected at the image plane in the exit port of the microscope. In this external interferometer, the image plane is optically Fourier transformed by lens L7 ($f = 7.5$ cm), and split into two separate beams by beam splitter BS. One of the beams (referred to as the reference beam) propagates toward pinhole P2 (diameter of 50 μm), which spatially filters the beam and erases the sample high spatial frequencies, mirror M5 reflects the filtered beam, and then lens L8 ($f = 7.5$ cm) Fourier transforms it back onto the camera plane. The other beam at the exit of beam splitter BS (referred to as the sample beam) is reflected back using retro-reflector RR, which shifts the center of the spatial-frequency domain. Because of this shift, the sample and reference beams interfere at a small angle on the CMOS digital camera (DCC1545, Thorlabs, with 1024×1280 square pixels, 5.2 μm each). The off-axis interference pattern recorded by the camera allows reconstruction of the wave front of the sample from a single exposure. Based on the interferometric projections obtained by the combined HOTs/IPM setup, TPM can be implemented.

The confocal fluorescent microscopy setup, used here just as a control experiment for the new label-free TPM approach, consists of 488/561 nm DPSS lasers, spinning disk (CSU-X1, Yokogawa), a half-upright microscope equipped with condenser/microscope objective C (Olympus LUMFI, 60×, NA = 1.10, water immersion), and an EM-CCD camera (iXon 897, Andor, with 512×512 square pixels, 16 μm each, and with single photon sensitivity). The confocal scan was performed by a piezoelectric scanner (Pifoc P-721.LLQ, Physik Instrumente, with 100 nm axial resolution). The confocal reconstruction was performed by IQ2 software (Andor).

We performed TPM of yeast cells (Saccharomyces Cerevisiae, longitudinal diameter range of 5–10 μm) in suspension during their reproduction by budding. Yeast cells are eukaryotic organisms that are helpful in noninvasive biological studies [21]. To hold and rotate the suspended cells by HOTs, we created two traps near the edges of cells along the y axis, as illustrated in Fig. 1. To achieve stable optical trapping, we used adaptive optics, changing the number and location of traps to optimize the trapping strength, even during cell rotation. The distanced two traps enabled a balanced rotation around the center of the cell. For TPM, we rotated the cell on the $y - z$ plane over 180° with angular steps of 5°, which is approximately an order of magnitude larger than the expected error of the trap localization, and defines the object rotation reproducibility.

At each step, an off-axis interferogram was captured using the external interferometric module. Several of these angular interferograms are shown in Fig. 2. The locations of the HOTs traps are illustrated by two red Xs in Fig. 2(a).

Following the acquisition, the complex wave front was digitally extracted from each off-axis interferogram by spatial filtering, obtained by cropping one of the cross-correlation terms in the spatial-frequency domain [14]. Next, a slight centering correction was performed based on the center of mass of the image. Then, the complex wavefront projections were processed digitally to create

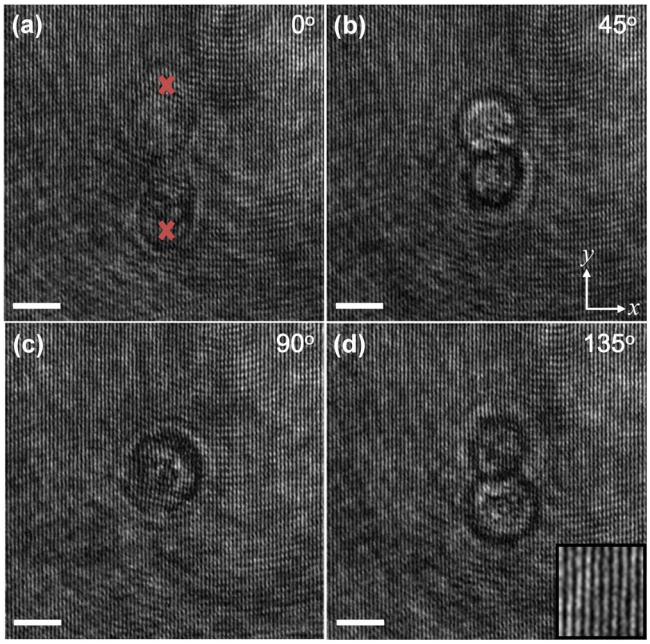

Fig. 2. Off-axis interferograms of yeast cells during 180° cell rotation obtained by HOTs, with 5° angular resolution. Examples for interferometric projections, taken at: (a) 0°, (b) 45°, (c) 90°, and (d) 135°. The inset in the bottom right shows a magnified area from the off-axis interference fringes at the background. The white scale bar represents 5 μm upon the sample.

the three-dimensional refractive index map of the cell by both the filtered back-projection algorithm and the diffraction theory algorithm [22]. Both reconstruction algorithms were implemented using Matlab. First, we defined the phase of the projection for the back-projection method and the Rytov field for the diffraction method, and performed a Fourier transform over it. Figures 3(a) and 3(b) show the results of the mapping of all projections on $k_y - k_z$ plane of the Fourier space based on the back-projection method and the diffraction method, respectively. As can be seen from Fig. 3, part of the Fourier space is not mapped in the diffraction method, as opposed to the back-projection method, because of the hemispheres that arise from the scattering of the waves. On the other hand, the diffraction method takes into consideration diffraction effects and does not simply

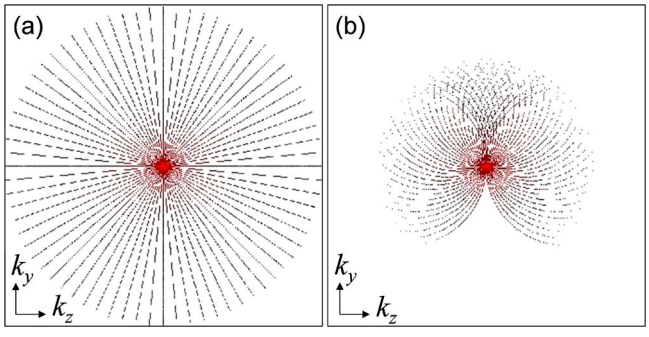

Fig. 3. Mapping of the $k_y - k_z$ plane of the Fourier space derived from all projections, as based on (a) the back-projection method, and (b) the diffraction method.

assume phase accumulation along straight lines, as assumed in the back-projection method. After mapping the projections to the Fourier space, a three-dimensional inverse Fourier transform is performed, and the refractive index is extracted according to the reconstruction method. The reconstruction process was performed offline and it lasted 32 s on 64-bit i5 CPU. Figure 4 shows these refractive index reconstructions, as obtained by the back-projection method [Figs. 4(a) and 4(b)] and by the diffraction method [Figs. 4(c) and 4(d)]. Media 1 and Media 2 show Z slicing throughout the reconstructed three-dimensional refractive index map planes, as obtained by the two reconstruction methods, whereas the central Z slice is shown in Figs. 4(a) and 4(c). The coinciding volumetric renderings from the two reconstruction methods, obtained by ImageJ, are shown in Figs. 4(b) and 4(d), and dynamic versions of these renderings are shown in Media 3 and Media 4. It can be seen that both algorithms present similar refractive index values of the inner cell contents, between 1.34–1.39, coinciding with the expected values for yeast cells [21]. The appearance of vacuoles, containing mostly water, is noticeable. It is also shown that the nucleus has wandered toward the spindle, which is one of the cellular steps in preparation for mother-daughter separation.

To validate our TPM results, a time series of confocal fluorescent images of yeast cells was obtained by the hybridized optical setup, as shown in Fig. 5. The yeast cells used expressed fluorescent proteins for the nucleus and cytoplasm (htb2-mCherry/spc42-YFP); thus, the nucleus fluorescent excitation/emission peaks were at 545/620 nm, and the cytoplasm fluorescent excitation/emission peaks were at 500/545 nm. The main steps in

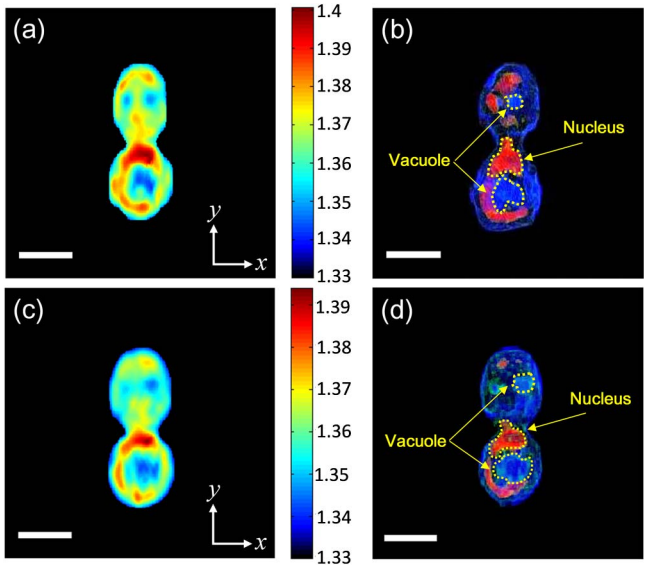

Fig. 4. TPM-based three-dimensional refractive index map of yeast cells obtained by (a), (b) the back-projection method, and (c), (d) the diffraction method. (a), (c) Central Z slice. See Media 1 and Media 2 for all Z slices. (b), (d) Volumetric renderings. See Media 3 and Media 4 for 3-D rotation animations. The background refractive index is $n = 1.33010 \pm 0.00047$. Note, however, that the background is not a part of the TPM, since it is not rotated with the cells. The white scale bar represents 5 μm upon the sample.

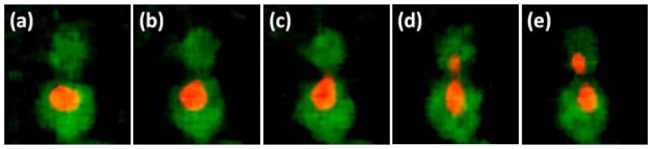

Fig. 5. Confocal fluorescent imaging of a yeast cell during division (central Z slices). The main steps are (a) bud appearance, (b) nuclear wandering toward the spindle, (c) nuclear division start, (d) absolute nuclear separation, and (e) mother-daughter separation. The label-free refractive index map shown in Fig. 4 was taken during stage (c).

yeast cell division include a bud appearance [Fig. 5(a)], nuclear wandering toward the spindle [Fig. 5(b)], transfer of DNA to the daughter cell [Fig. 5(c)], absolute nuclear division [Fig. 5(d)], and mother-daughter separation [Fig. 5(e)]. From Fig. 5, we learn that our TPM image, shown in Fig. 4 and acquired without using labeling, is taken during the nuclear division stage.

For TPM of yeast cells, stable rotation was obtained using a pair of traps located near the edges of the cell. Fewer than 100 mW were used per trap, inducing 1–2°C temperature rise, which is below the cell threshold damage. In general, the selection of the number and location of the optical traps is dependent on the particular cell structure to be rotated. Since biological cells are composed of many organelles, each possessing a slightly different refractive index, when a cell is subjected to a pattern of optical traps, it adjusts its position to minimize the forces acting on it. For this reason, rotation of larger cells in suspension, such as human cancer cells, is more challenging than rotating yeast cells. In this case, we expect that a cross-shaped array of traps will have the best performance in trapping the cell during rotation. Another solution is using polymer beads with high refractive index that can be attached to the cell membrane and are strongly trapped by HOTs.

Regarding the acquisition time, in our case we performed manual savings, which took a couple of seconds per each rotation step. However, much faster capturing can be obtained with full synchronization between the SLM and the camera, which signifies the technique advantage in capturing cellular dynamics.

To evaluate the refractive index resolution, we used our HOTs-TPM setup to acquire 5 μm silica bead, and obtained a refractive index of $n = 1.45 \pm 0.0092$ with (y, z) and x spatial resolutions of 0.37 μm and 0.69 μm, respectively, as obtained by spatial derivation of the three-dimensional refractive index map.

To conclude, we presented a new close-to-common-path off-axis interferometric setup integrated with HOTs, for manipulating and rotating live cells in suspension over a 180° angular range by a digital control over the rotation angle, while capturing the cell wave front by IPM, and allowing its three-dimensional refractive index map reconstruction. By inspection of the three-dimensional refractive index distribution of cells in suspension, the proposed method can be useful for characterizing biological processes and cell transformations from healthy to pathological conditions.

This research was supported by the FP7 Marie Curie Career Integration Grant (CIG) No. 303559.

References

1. F. Charrière, F. Montfort, J. Kühn, T. Colomb, A. Marian, E. Cuche, P. Marquet, and C. Depeursinge, Opt. Lett. **31**, 178 (2006).
2. F. Charrière, N. Pavillon, T. Colomb, C. Depeursinge, T. J. Heger, E. A. D. Mitchell, P. Marquet, and B. Rappaz, Opt. Express **14**, 7005 (2006).
3. W. Choi, C. Fang-Yen, K. Badizadegan, S. Oh, N. Lue, R. R. Dasari, and M. S. Feld, Nat. Methods **4**, 717 (2007).
4. S. O. Isikman, W. Bishara, S. Mavandadi, F. W. Yu, S. Feng, R. Lau, and A. Ozcan, Proc. Natl. Acad. Sci. U.S.A. **108**, 7296 (2011).
5. K. Kim, H. Yoon, M. Diez-Silva, M. Dao, R. R. Dasari, and Y. Park, J. Biomed. Opt. **19**, 011005 (2014).
6. Y. Sung, W. Choi, C. Fang-Yen, K. Badizadegan, R. R. Dasari, and M. S. Feld, Opt. Express **17**, 266 (2009).
7. W. C. Hsu, J. W. Su, T. Y. Tseng, and K. B. Sung, Opt. Lett. **39**, 2210 (2014).
8. A. Kus, M. Dudek, B. Kemper, M. Kujawinska, and A. Vollmer, J. Biomed. Opt. **19**, 046009 (2014).
9. D. G. Grier and Y. Roichman, Appl. Opt. **45**, 880 (2006).
10. M. Yevnin, D. Kasimov, Y. Gluckman, Y. Ebenstein, and Y. Roichman, Biomed. Opt. Express **4**, 2087 (2013).
11. M. K. Kreysing, T. Kiebling, A. Fritsch, C. Dietrich, J. R. Guck, and J. A. Kas, Opt. Express **16**, 16984 (2008).
12. P. Girshovitz and N. T. Shaked, Biomed. Opt. Express **3**, 1757 (2012).
13. N. T. Shaked, Opt. Lett. **37**, 2016 (2012).
14. P. Girshovitz and N. T. Shaked, Opt. Express **21**, 5701 (2013).
15. N. Cardenas and S. K. Mohanty, Appl. Phys. Lett. **103**, 013703 (2013).
16. T. Yasokawa, I. Ishimaru, M. Kondo, S. Kuriyama, T. Masaki, K. Takegawa, and N. Tanaka, Opt. Review **14**, 161 (2007).
17. T. Kozacki, R. Krajewski, and M. Kujawinska, Opt. Express **17**, 13758 (2009).
18. B. Kemper, A. Barroso, M. Woerdemann, L. Dewenter, A. Vollmer, R. Schubert, A. Mellmann, G. V. Bally, and C. Denz, J. Biophotonics **6**, 260 (2013).
19. P. Memmolo, L. Miccio, F. Merola, O. Gennari, P. A. Netti, and P. Ferraro, Cytometry, Part A **85**, 1030 (2014).
20. F. Merola, L. Miccio, P. Memmolo, M. Paturzo, S. Grilli, and P. Ferraro, IEEE Photon. J. **4**, 451 (2012).
21. B. Beauvoit, H. Liu, K. Kang, P. D. Kaplan, M. Miwa, and B. Chance, Cell Biophys. **23**, 91 (1993).
22. A. C. Kak and M. Slaney, *Principles of Computerized Tomographic Imaging* (IEEE, 1988).